

# Solidification of leads: Theory, experiment, and field observations

J. S. Wettlaufer

Applied Physics Laboratory and Department of Physics, University of Washington, Seattle

M. Grae Worster and Herbert E. Huppert

Institute of Theoretical Geophysics, Department of Applied Mathematics and Theoretical Physics  
University of Cambridge, Cambridge, England

**Abstract.** Thin sea ice plays a central role in the surface heat and mass balance of the Arctic Ocean. In order to develop understanding of these balances we describe and analyze highly resolved temperature data taken through the air/sea/ice interface during the transition from an ice-free to an ice-covered Arctic Ocean surface. The data were taken to observe the thermodynamic evolution of a lead, a process that has previously only been accessible to measurement techniques confined to the lead edge. Our detailed analysis of the field data is guided by recent theoretical and experimental advances in understanding the phase dynamics of directionally solidified alloys. Because of the dearth of direct observations we also present time series of the relevant heat fluxes inferred from our data and demonstrate the controlling influence that the internal phase evolution has on these quantities. We have previously examined the stability of the brine trapped in a growing sea ice matrix both theoretically and experimentally and now find that haline convection, driven from within the growing layer, is consistent with this previous work and with the nature of direct turbulence measurements. The importance of this process is that although ice growth is continuous, the local brine flux commences abruptly, only after some time, in contrast to what had previously been supposed. Hence the ice growth process itself is a source of intermittency in oceanic boundary layer turbulence. Furthermore, we find that in this particular situation the sea ice growth is not simply a square root function of time, in contrast to the model typically used in numerical simulations. By far the most practical methods of studying lead convection are numerical simulations and laboratory models, and a strong conclusion of this study is the importance of the proper treatment of the boundary conditions describing the buoyancy flux.

## 1. Introduction

The divergence of wind stress continually produces cracks in the perennial sea ice cover known as leads. These transient fissures attract scientific attention because they provide a thermal conduit through which heat and radiative transfer processes are enhanced tremendously, relative to the thick pack ice that surrounds them. The thermal importance of leads was put in context by *Badgley* [1966], who showed that during winter the atmospheric heat flux from rapidly freezing leads can be several orders of magnitude larger than that over perennial sea ice, 3–4 m thick. He emphasized the large-scale implications of leads by arguing that they need occupy only ~1% of the area of the ice cover in order to dominate the exchange of heat from the ocean to the atmosphere. Model calculations by *Maykut* [1978, 1982] bear out the work of *Badgley* and show April to be the dominant month with respect to the role of thin ice in the surface heat balance. *Maykut* found that when 1% of the Arctic Ocean is covered by leads, the volume of wintertime ice production within them is equivalent to that of the remaining 99% of the perennial ice pack. Rapid solidification at lead surfaces significantly influences the ther-

mohaline structure of the ocean; an even less practicably accessible component of the air/sea/ice system. As was discussed by *Malmgren* [1927], and most likely known to Inuits long before, sea ice formed in its first growth season is, in bulk, much less saline than the ocean from which it formed. The combination of this fact, along with modeling and field studies, shows that the solidification of leads is a significant source of buoyancy forcing for the Arctic Ocean. Because general circulation model (GCM) studies are sensitive to convective parameterization schemes that treat salt rejection during ice growth [e.g., *Duffy et al.*, 1999] and because the scale of a lead is typically much smaller than a GCM grid cell, the link between vigorous local convection and large-scale hydrography is an active field of inquiry.

The evidence from *Maykut's* [1982] numerical modeling studies of a strong link between the two is compelling. He found that if young ice is not included in the salt budget, the salinity of the mixed layer would not increase significantly until early December. However, the mixed layer has a seasonal signal that begins to evolve many months prior to this [*Morison and Smith*, 1981], which suggests that the local salt production in leads is redistributed on a large scale. Concurrent observations of the brine evolution of rapidly growing thin ice and the accompanying salt fluxes that are produced in the ocean have, until recently, been unavailable. Therefore the hypothesis that

Copyright 2000 by the American Geophysical Union.

Paper number 1999JC900269.  
0148-0227/00/1999JC900269\$09.00

leads, through their intense brine production and associated thermohaline convection, are central to the establishment of the large-scale water mass characteristics in the Arctic Ocean led the community to stage a field campaign [*The LeadEx Group*, 1993]. This paper is centered on observations, made during that program, of rapid solidification in a lead during the initial stages of evolution. The data are analyzed within the context of our previous work on the theory of two-component, two-phase mixtures and a suite of laboratory experiments designed to simulate the important physical mechanisms at play in the natural environment. The field observations bear out the essential features of those simulations and compare favorably with oceanographic measurements. The central message of this paper is that the majority of the dense brine formed during the early stages of freezing remains trapped within the interstices of the crystalline matrix until a critical thickness is reached. This is the thickness at which the potential energy owing to the density drop across the intercrystalline fluid is just sufficient to overcome the viscous dissipation resulting from any fluid motion. At greater thicknesses, disturbances release the dense fluid from the interior of sea ice and drive haline convection in the ocean below. Hence the salinity flux is not initiated when ice growth begins but occurs abruptly after the ice has reached a critical thickness, which depends on the temperature difference across the ice layer. There are several important consequences of this effect. First, although ice growth is continuous at a given location, the brine flux is not directly proportional to the growth rate for all stages of growth, although the latter has generally been supposed. Such proportionality is not reached until considerably after the onset of the instability that releases the intercrystalline brine, a delay which can be greater than half an inertial period. Second, because of the horizontal distribution in the ice thickness, there will be an associated distribution in critical conditions, which weds the ice growth process itself to intermittency in the turbulence in the oceanic boundary layer. Third, we found, at least in this instance, that during the very early stages of its evolution, the time dependence of the surface temperature resulted in an ice growth rate that was virtually constant, in contrast to the model typical used in simulations. We conclude that boundary conditions for both laboratory and numerical simulations of haline convection under leads need to account for such time-dependent effects. An understanding of these local processes is necessary to develop physically based parametrization schemes of ice growth processes in large-scale models.

## 2. Lead Experiment

The Lead Experiment field campaign consisted of a pilot experiment during April 1991 and the main program which began on March 12, 1992, with the establishment of a base camp in the Beaufort Sea at 72°47'N, 147°W. A detailed description of the logistics, scientific program, and the few previous field efforts has been given by *The LeadEx Group* [1993]. We briefly outline the relevant aspects of the field program here. The strategy relied on daily helicopter reconnaissance to survey an area, centered on the main camp, for recently formed leads. When a suitable lead was found, huts fitted out with scientific and living equipment were transported by helicopter to the site. Atmospheric, oceanographic, and ice programs were deployed at the lead site for between 2 and 4 days. There were four main lead deployments during the 6-week main experiment. Typical conditions included surface air tem-

peratures between -25°C and -15°C, strongly diurnal short-wave radiation and winds rarely exceeding 12 m s<sup>-1</sup>. A particularly interesting deployment is "lead 3" which was the largest lead. The ice velocity varied from 11 to 13 cm s<sup>-1</sup>, about an order of magnitude greater than that of lead 4 which has also been studied [*Morison and McPhee*, 1998]. The size and forced convective regime of lead 3 make it particularly interesting, and for this reason there has been more treatment of it in the literature. Deployment at lead 3 began early on the morning of April 6 and was evacuated 2 days later. At the time of deployment the lead was located at 72°45'N, 144°50'W and was approximately a kilometer wide. A photograph of this lead at the initiation of evacuation is shown by *The LeadEx Group* [1993]. With the exception of the program investigating the atmospheric boundary layer, the scientific teams were located on the upwind side of a lead because, with respect to a reference frame fixed to the ice, the upwind edge is typically downstream with respect to the ocean currents. The influence of rapid ocean freezing on the oceanographic boundary layer is best studied by observing downstream oceanographic profiles which must therefore be done from the upwind edge of the lead.

In addition to the logistical burden of studying the early stages of lead development, there is an obvious measurement problem: one must typically wait until the ice is 6 cm or more thick before venturing too far from the lead edge. *Gow et al.* [1990] made measurements of structural and physical properties in a relatively small lead during the Coordinated Eastern Arctic Experiment drift phase. They made clear that the proximity of the perennial ice, and the associated wind-blown snow, was largely responsible for the high percentage of granular ice in the surface of the lead, which is in contrast to the observational evidence that granular ice constitutes a minute fraction of the central Arctic sea ice cover. In the ~1 km wide lead 3 that we are focusing on here, conditions were more typical in that, except for the canonical edge effects where anomalous properties associated with the buildup of frazil ice were observed [*Perovich and Richter-Menge*, 1994], congelation ice growth began in the first 1 cm.

## 3. Instrumentation

Instrumentation for the field campaign was developed at the Applied Physics Laboratory (University of Washington) for deployment directly into the ice-free water of a newly formed lead. The goal was to monitor the evolution of the temperature field normal to the air/sea interface during the initial stages of ice formation, well away from edge effects that dominate attempts to monitor the system from the platform of the pack ice. Furthermore, because of the relatively delicate nature of the initial ice skim, a nondestructive approach was necessary. The instrument (Figure 1a) is a cylindrical polyvinylchloride buoy, embedded in the wall of which is a vertical array of thermistors spanning 98 cm. We calibrated the array for each buoy independently to ±0.05°C using the Pacific Northwest Calibration Laboratory facilities. Thermistors are known to drift over long periods of time, especially in extreme environments. We did not perform postdeployment calibrations but instead employed in situ corrections using independent measurements of temperature and salinity in the water column (T. Stanton, personal communication, 1999). The buoy housing has a diameter of 25 cm, a choice which was based on several factors. It was desirable that the instrument did not drift substantially in the surface wind-wave field, and hence it required

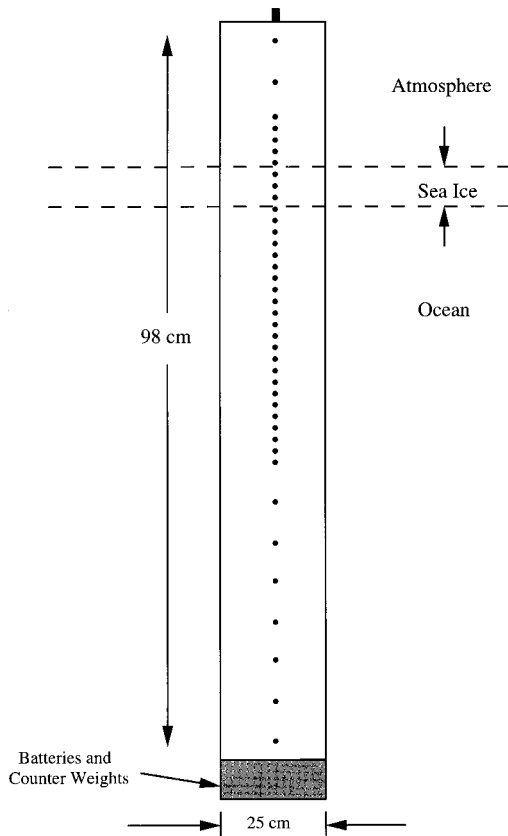


**Figure 1a.** A schematic diagram of the freeze-in-buoy. The cylindrical housing contains 41 thermistors; the top three thermistors are separated by 4 cm; thermistors 3 through 33 are separated by 2 cm; and 4 cm separate thermistors 33 through 40. Depending on the buoy, the seventh or eighth sensor from the top was at the water line. The base of the housing contains counterweights and batteries to maintain stability and the proper level of buoyancy, and an internal frame supports the electronics boards and wire junctions. Any remaining air space was filled with styrofoam packing material to suppress thermal convection. The data were stored internally on EPROM, which could be interrogated using RS232 cable and a personal computer after the ice was thick enough to bear weight. The sampling interval for all the data reported here is 1 min.

an internal diameter that provided sufficient counterweighting for low-frequency buoyancy behavior. A cross section that was too large, however, would create oscillations that would prevent it from being frozen into the ice. The housing also had to be large enough to contain the electronics package and batteries. We required that it extended sufficiently deeply into the water column to provide a stable temperature for the reference electronics which were just above the counterweights and batteries. Data were stored on internal memory, which could be interrogated using RS232 cable and a personal computer after the ice was thick enough to bear weight. The sampling interval for all the data reported here was 1 min.

Because the instruments could be moved by one person, they were ideal for rapid deployment. A typical deployment scenario is as follows. The buoys were programmed to begin sampling at the base camp and then loaded into the helicopter before the reconnaissance flight. If a suitable lead was found, deployment began immediately. A gimbed collar was attached to the buoy into which a light weight extendable “window-

washer” pole was inserted. The buoy was placed in the water at the edge of the lead and then pushed well away from the edge (5 m or more) by extending the pole system. Tethers were attached to each side of the collar and run back to the lead edge to maintain the pole system normal to the lead edge (see Figure 1b). Three buoys were deployed in this manner from the upwind, or downstream, side of each lead. The boundary layer dynamics at lead 4 were substantially weaker than at lead 3, reaching background geostrophic levels within a few hours of deployment [McPhee and Stanton, 1996]. Therefore the oceanographic response of ice growth was less interesting in lead 4 than it was in lead 3, which is why we focus on the latter in this paper.

#### 4. Basic Observations

We measured the temperature at each sensor every minute. Because a buoy often remained on the ice surface for some time before deployment, there was a transient period immediately after deployment during which the submerged fraction of the instrument warmed to the ocean temperature. Although the majority of the buoy was submerged,  $\sim 30$  cm was in the atmosphere, which resulted in a slow change in the temperature due to heat conduction down the cylindrical shell. Since the latter is a thermal insulator relative to the ice, this effect is much slower than the temperature variations we are measuring, typically  $\sim 0.01$  mK min $^{-1}$ , and hence straightforward to correct. Essentially all of our analysis derives from these temperature data. We use them to estimate the temperature gradient and the position of the ice/ocean interface as a function of time. We also use the temperature data, combined with theoretical considerations, to estimate conductive and latent heat fluxes during the solidification process, and hence we focus only on the data in a region near the air/sea/ice interface.

There are two revealing methods of extracting the ice thickness from the temperature data. We discuss these with reference to Figure 2 in which we plot the temperature-time traces from both of the buoys that were deployed late on the afternoon of April 6, 1992. Buoy 5 was deployed  $\sim 2$  hours before buoy 6. During a time interval that we denote as  $t_{eq}$ , the submerged sections of the buoys warm to the ocean temperature, which is barely discernible on the scale shown in Figure 2. We cannot begin to extract information concerning the ice growth until  $t_{eq}$  is reached for each buoy. Because buoy 5 was deployed first, we measure time in minutes relative to  $t_{eq}$  for buoy 5. The additional timescale is decimal days of 1992, abbreviated as UT, in which the time origin in minutes corresponds to 0221, day 98 UT. The temperature-time trace of the coldest thermistor is that corresponding to the ice/atmosphere interface. As will be discussed below, the observed diurnal variation in solar insolation, with two peaks during the  $\sim 2.8$ -day deployment, has a controlling influence on both the heat and mass budgets of the evolving air/sea/ice system.

We can “directly” observe the growth of sea ice as it engulfs an increasing fraction of the buoy. The downward motion of the sea ice/ocean interface is observed by plotting the vertical temperature profile as a function of time. The interface between cold sea ice and the warm isothermal ocean can be delineated at any time from the discontinuity of the temperature gradient. Therefore the downward motion of the discontinuity is a measure of the growth of the sea ice.

In Figure 2c we plot profiles between the surface, at zero depth, and 16 cm below from buoy 6 at lead 3. The initial



**Figure 1b.** Photograph of the deployment (see text for detail).

profile was taken after the buoy had reached the oceanic temperature, and each subsequent profile is separated by 200 min. A quantitative analysis of this form of the temperature data is, however, rather inaccurate, and it is particularly difficult for the thin ice we are studying. One must find the interface by intersecting two curves: the temperature profile through the ice and that through the water column. The principle difficulty with this method is that it is sensitive to the fitting procedure for the temperature gradient in the ice, and for thin ice the error in the intersection point is of order the ice thickness itself. Over much longer timescales such a method might be suitable, but it was not sufficient for our purposes.

A much more reliable method involves the analysis of temperature-time traces from each thermistor. To illustrate the method, in Figure 2d we plot the temperature history of six thermistors between the ice surface and 10 cm below, beginning at the time of deployment. Initially, the buoy warms to the ocean temperature. After the solidification front passes a sensor the sensor begins to cool rapidly. Those that remain in the water column are, on the timescale of 1 min, at the equilibrium melting point determined by the salinity. Therefore we can estimate the growth rate of the ice layer by observing the time at which a given sensor reaches the freezing temperature, an idea quantified in the algorithm discussed presently.

An algorithm was developed to use the traces of time against temperature in order to compute the times at which a given thermistor is engulfed by growing sea ice. We record the time at which a sensor reaches a temperature that is less than the equilibrium melting temperature by an amount  $\epsilon$ , which was taken to be as small as possible and was never larger than  $0.25^{\circ}\text{C}$ . It is necessary to wait for a measurement that is less than the freezing temperature by an amount that is greater than the small temperature fluctuations resulting from convection and other fluid motions. Since we know the position of each thermistor, this criterion provides an estimate for the depth of the layer at that time. We then fit these estimates by regression, thereby producing a continuous curve of depth against time. The error of this estimate is systematic insofar as we know that by the time the temperature of a sensor is  $\epsilon$  less

than the melting temperature, the actual interface has moved a little distance below it. An additional, albeit subtle, influence on our ability to estimate the interface position is the fact that near the ice/ocean interface the volume fraction of brine is large and the local temperature gradient is weak. Hence, overall, we expect the algorithm to underestimate the thickness.

The method was therefore tested using laboratory experiments in which the growth rate was measured independently [Wettklauser *et al.*, 1997a, b]. In Figure 3 we show two plots of the height of the ice formed in the laboratory during the directional solidification of a 35.5 practical salinity unit (psu) (parts per thousand) sodium chloride solution from a boundary with a constant temperature. The method does indeed systematically underestimate the ice thickness, but the offset is within the measurement error of the depth. Therefore we are confident that the method reliably reproduces the ice growth rate from the temperature data.

We used this procedure to obtain estimates of the ice growth rate at lead 3 as derived from buoys 5 and 6, which were separated by  $\sim 25$  m along the lead. These estimates are shown in Figure 4, with the initial offset due to the difference in the time of deployment. Note that the growth rates at the two buoys are the same to within ten percent. Furthermore, the estimates agree to within 1 cm on the final thickness observed at the time the buoys are recovered. Note also that relative to the sort of growth measured in the laboratory experiments (Figure 3), the growth rate in the first 12 hours is more nearly constant.

In section 5 we provide a simple argument for this observed constant growth rate during this early time interval. In section 6 we show that the form of the growth during this early time is crucial for understanding the brine flux evolution.

## 5. Heat Fluxes

Maykut [1978] performed numerical calculations of the heat balance over young sea ice. In his studies he calculated the heat budget for ice of various thicknesses but did not study the time dependence of the energy balance as the ice grew. He pointed

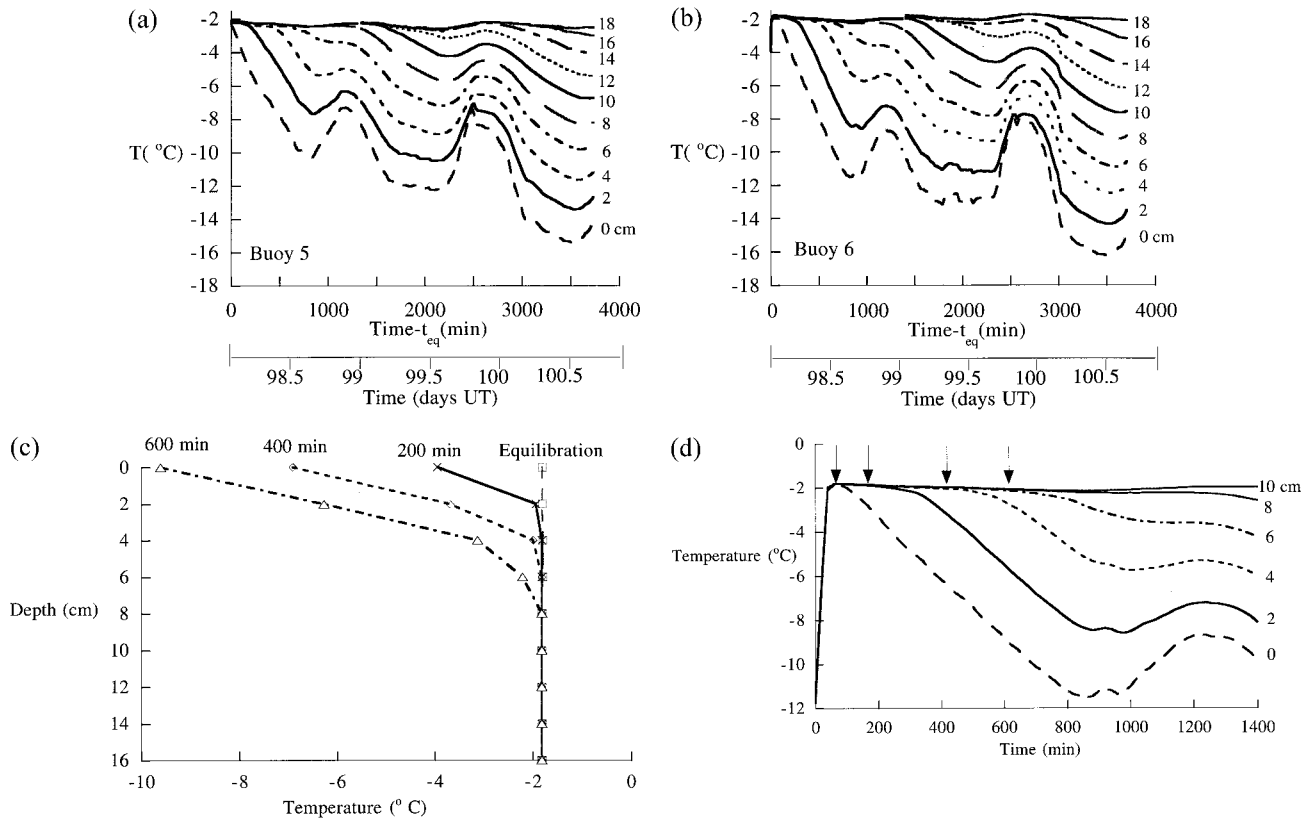


**Figure 2.** Temperature-time traces from (a) buoy 5 and (b) buoy 6 at lead 3 deployed late on the afternoon of April 6, 1992. The depths of the sensors corresponding to each trace are indicated on the right-hand side, with the coldest thermistor corresponding to the ice/atmosphere interface at 0 cm. Buoy 5 was deployed  $\sim 2$  hours before buoy 6. During a time interval  $t_{eq}$ , the submersed sections of the buoys warm to the ocean temperature. The timescale used by the LeadEx investigators is decimal days of 1992, abbreviated as UT and denoted on the figure. The time origin in minutes corresponds to 0221, day 98 UT. (c) The discontinuity in the vertical temperature profile delineating the interface between cold sea ice and the relatively warm isothermal ocean. These profiles between the surface, at 0 cm, and 16 cm below were obtained from buoy 6 at lead 3. The initial profile was taken after the buoy had reached the oceanic temperature, and each subsequent profile is separated by 200 min. A quantitative analysis of this form of the temperature data is rather inaccurate (see text), and it is not suitable for our purposes. (d) Blowup of the temperature-time traces using six thermistors between the ice surface and 10 cm below from buoy 6 with the time origin being that of deployment. The growth rate of the ice layer is estimated by observing the time indicated by the arrows at which a given sensor reaches a temperature slightly less than the freezing point.

out the complicated brine volume evolution expected during the growth of young sea ice. However, as is consistent with separate time-dependent calculations, he specified the salinity structure of the ice and under these circumstances found a linear temperature profile through young ice  $< 30$  cm thick. He therefore approximated the conductive heat flux through the ice as the product of the temperature gradient across the entire depth and Untersteiner's [1961] approximate relation for the temperature and salinity-dependent thermal conductivity of sea ice evaluated at the ice surface. This represents the net amount of heat entering the atmosphere through the ice, which is subsequently partitioned between radiative, sensible, and latent heat fluxes. He calculated the energy budget for open water, 5 cm, and 10 cm (and thicker) sea ice each month except for July and August. For April he found that  $\sim 60$  times more heat is lost from 5-cm ice than for perennial ice 3 m in thickness. Such dramatic differences have been one of the primary motivations in the study of leads and partly responsible for the choice of spring for the lead experiment.

### 5.1. Solid Fraction and Brine Volume

Our temperature measurements are relevant to the highest heat flux region of Maykut's [1978] calculations, which occur between 0 and 5 cm of ice cover. In the sea ice literature the most common quantity used to characterize the volume of salts in the material is the brine volume [e.g., Cox and Weeks, 1988]. To calculate it, one needs to know the temperature and salinity of a sample. We prefer to work with the solid fraction  $\phi$ , which is the volumetric fraction of ice in the sample (some eutectic temperatures are reached, but the mass of solid salts in the ice will be insignificant in relation to the mass of ice). Although the solid fraction is simply related to the brine volume, it has the advantage of having a precise interpretation within the theory of "mushy layers" [Worster, 1992a], upon which our analysis is based. These arise because when a multicomponent system solidifies, it generally forms a mushy layer, which is a technical term (coined by metallurgists) for a solid matrix bathed by interstitial fluid (generally of different composition).

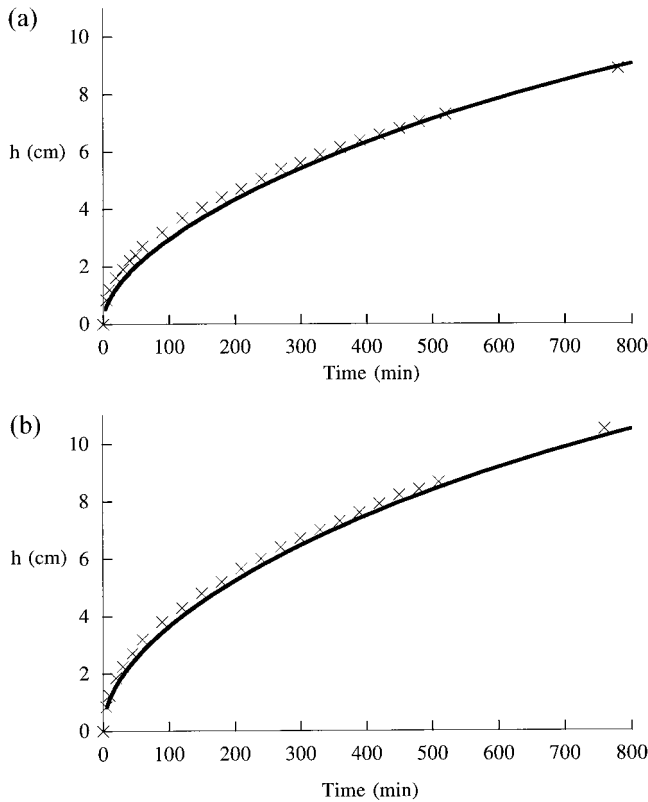


**Figure 3.** A test of the ice thickness algorithm using laboratory experiments in which the growth rate is measured independently. Plots of the thickness of the mushy layer formed during the directional solidification of a 35.5 psu sodium chloride solution from a boundary at a constant temperature of (a)  $-15^{\circ}\text{C}$  and (b)  $-20^{\circ}\text{C}$  for a period of  $\sim 13$  hours. The observed thickness is plotted as crosses, and the solid curve is the thickness predicted solely by analysis of the temperature data using the algorithm described in the text. The value of  $\varepsilon$  used here is  $0.15^{\circ}\text{C}$ . Both curves are within the measurement error and systematically underestimate the thickness for the reasons described in the text. Note that the curve does not begin at the origin because the first thermistor to be engulfed is at a depth of 1 cm.

There are many different natural and industrial examples of mushy layers, and by this technical definition, sea ice can be considered as a mushy layer. For the remainder of this paper we will use the terms sea ice and mushy layer interchangeably. We note here that in the sea ice community the lowermost region of an ice sheet, known as the “skeletal layer” [Weeks, 1998], is recognized as the region with the highest brine volume and the least mechanical strength. Hence, intuitively, one might equate the skeletal layer with the mushy layer, and indeed, for very thin ice, they may be commensurate. However, by definition a mushy layer accommodates the entire thermodynamic range of a system and hence is a concept that can be used to describe the entire thickness of a growing ice sheet.

Clearly, throughout a growing ice sheet the brine volume adjusts to changes in temperature and so too does the solid fraction. The causes are the same: the growth or melting of ice crystals in response to local changes of temperature and salinity. Even under ideal conditions, in the presence of interstitial fluid flow a rigorous predictive model for how the material adjusts to these changes is extremely complicated and nonlin-

ear (see Worster [1997] for a recent review). Significant predictive capability for the temperature, salinity, and solid fraction fields is possible when these adjustments occur rapidly in order to maintain the two-phase region everywhere in local thermodynamic equilibrium.

Within the sea ice matrix the local salinity of the liquid phase  $S$  and the local temperature  $T$  are related to one another through the phase diagram for sea ice [e.g., Weeks, 1998; Wettlaufer, 1998]. The thermodynamic term for the curve that defines the salinity dependence of solid-liquid coexistence at constant pressure is the “liquidus” which we denote here as

$$T = T_L(S). \quad (1)$$

In oceanographic parlance this is simply the salinity-dependent freezing point of seawater, and in the range of salinities encountered here we assume that the equilibrium phase diagram is linear  $T_L(S) = mS$ , where  $m = -0.05236 \text{ K psu}^{-1}$ . The phase evolution of sea ice is largely characterized by the space-time variation in  $\phi$ , which determines the internal release of latent heat within the system and thereby influences the overall growth rate of the layer and its long time microstructural evolution and desalination [Wettlaufer et al., 1997a, b; Worster and Wettlaufer, 1997]. If we assume that the local solid-liquid coexistence is determined by (1), then the “lever rule” [e.g., Kurz and Fisher, 1984] can be used to infer  $\phi$  if the local temperature and the bulk composition are known. The lever rule provides a relationship between solid fraction and the local salinity of the interstitial brine and follows from an assumption of complete local equilibrium throughout an element that contains both solid and brine. The ice lattice is extremely efficient in its segregation of impurities, and hence for most aqueous solutes the local distribution coefficient  $k$  (defined by  $S_s = kS$ , where  $S_s$  is the salinity of the ice) is very small;  $k \leq 10^{-4}$  [Gross et al., 1987]. Therefore the solid phase is nearly

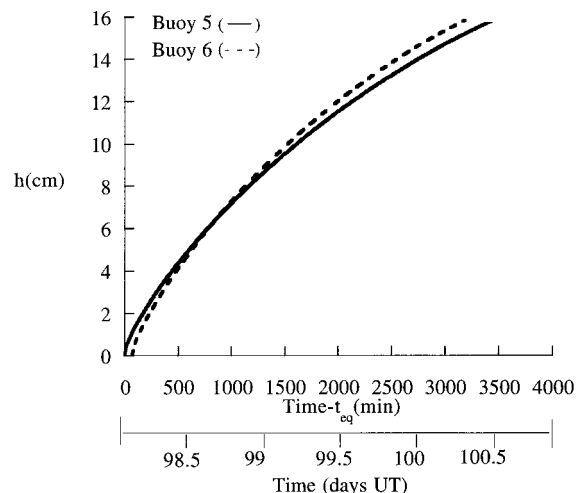


**Figure 4.** Plots of the estimates of ice thickness as derived from buoy 5 (solid curve) and buoy 6 (dashed curve) at lead 3. The value of  $\varepsilon$  used is  $0.25^{\circ}\text{C}$  because the cooling rate of the ice formed in the field is smaller than that observed in the laboratory where the surface boundary condition is maintained at a constant low temperature. When the buoys were recovered, the ice thickness was measured directly to be  $18 \pm 0.5 \text{ cm}$ . The text describes the origins of different temporal growth exponents.

pure ice. The bulk salinity of an element of sea ice is then given by

$$\bar{S} = (1 - \phi)S. \quad (2)$$

The lever rule, which follows from rearrangement of (2), can immediately be written as

$$\phi = 1 - \frac{\bar{S}}{S}. \quad (3)$$

If, as we shall show in section 6, all of the impurities rejected by the ice lattice are initially retained within the interstices of a layer of sea ice, then during that time the bulk salinity of an element is equal to that of the ocean from which it came and  $\bar{S} \equiv S_0$ . Under the assumptions leading to (3) the local salinity is constrained to the liquidus, so that if we know the local temperature as a function of depth  $z$ , then we know the local salinity  $S(z) = m^{-1} T(z)$ . Hence equation (3) can be expressed as an equation for the local solid fraction in terms of observable quantities through

$$\phi = 1 - \frac{mS_0}{T(z)}. \quad (4)$$

For some purposes we are interested in global (here meaning depth averaged) heat balances, and hence self-consistent estimates must be made for the solid fraction. We are also able to obtain the depth averaged solid fraction  $\bar{\phi}$  from observable quantities. Here we assume that the solid fraction is independent of depth and apply global mass balance at each time, and hence at each sea ice thickness  $h$ , which leads to

$$S_0 h = (1 - \bar{\phi}) \int_0^h S(z) dz, \quad (5)$$

from which

$$\bar{\phi} = 1 - \frac{mS_0 h}{\int_0^h T(z) dz}. \quad (6)$$

There are various degrees of sophistication that can be implemented when applying (6) to our data, and in some cases the data only warrant the simplest treatment. Under the assumption of a linear temperature profile we need only know the ice depth  $h$  and the surface temperature,  $T(z=0) \equiv T_0$ , in which case the integral in (6) is  $0.5[T_0 + T_L(S_0)]h$ . However, since we have also estimated the depth at each time, we can fit the temperature profile through the layer to a quadratic function at each time,  $T(z) = a(t) + b(t)z + c(t)z^2$ , for which (6) can also be integrated directly. Clearly, the quadratic function cannot be used until the interface has passed the second thermistor. In our laboratory work we have assumed a linear temperature gradient in the estimates of  $\bar{\phi}$ , but for the field data we use the quadratic form for all ice depths  $>4$  cm.

## 5.2. Heat Fluxes

Mushy layers have thermal properties intermediate between those of the individual phases. Because the ice platelets are principally oriented parallel to the local heat flux vector, the local thermal conductivity for vertical heat transfer in sea ice is well approximated by

$$k = k_i \phi + k_w (1 - \phi), \quad (7)$$

where  $\phi$  is the local solid fraction and  $k_i$  and  $k_w$  are the thermal conductivities of ice and water, which we take to be 2.03 and 0.56 W m<sup>-1</sup> K<sup>-1</sup>, respectively, although they have a weak temperature dependence in the range of relevance here. Given the mean solid fraction  $\bar{\phi}$  defined above, we assume that the mean conductivity similarly takes the form

$$\bar{k} = k_i \bar{\phi} + k_w (1 - \bar{\phi}). \quad (8)$$

The conductive heat flux  $F_c$  can then be evaluated either locally or as a depth average by multiplying either (7) or (8) by the appropriate temperature gradient.

Because the temperature and salinity, and hence the solid fraction, vary with depth, the net latent heat flux associated with sea ice growth is manifested at the ice surface as a conductive heat flux. The continuous internal solidification that occurs as the ice cools manifests itself as a time variation of  $\bar{\phi}$  (see section 6). Since it is the cooling of the ice that conducts heat away and allows further solidification to occur, we write the mean latent heat flux as

$$\bar{F}_\ell = \bar{\phi}(t) \rho_i q_m \dot{h}, \quad (9)$$

where  $\rho_i = 917$  kg m<sup>-3</sup> and  $q_m = 3.35 \times 10^5$  J kg<sup>-1</sup> are the density and latent heat of fusion for pure ice and  $\dot{h}$  denotes the sea ice growth rate.

During the initial cooling period we can illustrate the nature of the growth rate as follows. Figure 2d shows that for the first 800 min,  $T_L(S_0) - T_0$  increased linearly with time. If we fit this data with a straight line, we find that  $T_L(S_0) - T_0 = At$ , with  $A = 1.28 \times 10^{-2}$  K min<sup>-1</sup>. In section 6 we discuss the observed evolution of  $\bar{\phi}$ , and fitting these data similarly over the first 800 min yields a coefficient  $B = 2.23 \times 10^{-3}$  min<sup>-1</sup>.

The complete balance of energy that controls the evolution of the depth of the mushy layer is that between the release of latent heat, the conductive heat flux through the layer to the atmosphere, and the turbulent oceanic heat flux at the underside of the ice. As described in section 5.1, the reliability of our conductive heat flux calculations increases after 2 cm of ice has formed and a second thermistor has been engulfed. However, independent direct measurements of the turbulent ocean heat flux at early times [McPhee and Stanton, 1996, Figure 11b], and our estimates after  $\sim 400$  min, are consistent with the principal balance controlling the depth of the mushy layer as that between the release of latent heat and heat conduction. Thus we can write

$$\bar{\phi}(t) \rho_i q_m \dot{h} = \bar{k} \frac{At}{h(t)}, \quad (10)$$

which leads to the following relationship:

$$\rho_i q_m h^2 = \frac{1}{2} (k_i - k_w) At^2 + k_w \frac{A}{B} t. \quad (11)$$

The result demonstrates that depending on the rate of surface cooling (embodied in the coefficient  $A$ ) and evolution of phase change internal to the mushy layer (embodied in the coefficient  $B$ ), the overall thickness may increase linearly with, or as the square root of, time. Therefore it is not obvious a priori that a particular growth law is dominant, as has generally been supposed, and hence the complete suite of conservation equations of the theory of mushy layers must be implemented.

In Figure 5 we plot the latent and conductive heat fluxes

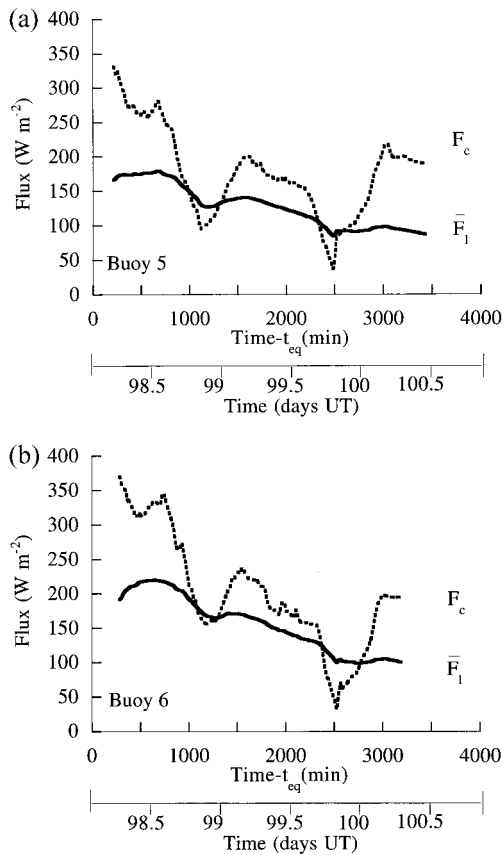


**Figure 5.** Plot of the estimates of conductive (dotted line) and latent heat (solid line) fluxes derived from the temperature data from (a) buoy 5 and (b) buoy 6 at lead 3. The conductive heat flux is calculated as that at the ice surface using the local model described in the text. Note that the two diurnal heating intervals seen in Figure 2 have the obvious consequence of a reduction in the conductive heat flux and concomitant reduction in the latent heat flux.

from lead 3 as derived from buoys 5 and 6. The conductive heat flux is evaluated at the surface using the local solid fraction and conductivity (equations (4) and (7)). A striking result is the observed spatiotemporal variation in the fluxes along the lead. Although the growth rates and ice thicknesses (Figure 4) are very similar (the difference in ice thickness during this period is never  $>1$  cm), the heat balance varies substantially during the first half of the deployment. The individual maxima of the conductive heat fluxes are  $327 \text{ W m}^{-2}$  for buoy 5 and  $370 \text{ W m}^{-2}$  for buoy 6, and the mean and maximum differences between the two locations are  $25 \text{ W m}^{-2}$  and  $75 \text{ W m}^{-2}$ , respectively. We believe that most of this spatial variation originates from the fact that the phase evolution of sea ice is strongly history-dependent and hence the difference in time evolution of its solid fraction profile (as shown later in Figure 8) can significantly influence the energy budget. Notwithstanding the drops owing to solar radiation, the solid fraction does not vary significantly in time after its initial increase, which is in qualitative agreement with our laboratory studies [see Wettlaufer *et al.*, 1997b, Figure 17]. The largest flux in the energy balance for thin ice is  $F_c$ . Hence it is relevant to compare our estimates with Maykut's [1978] calculations of the conductive heat fluxes for 5-cm-thick sea ice. On the first day of March, April, and May he found  $F_c$  to be 494, 401, and  $176 \text{ W m}^{-2}$ , respectively.

The small-scale spatial variability in  $F_c$  that we have observed, with a maximum difference of  $75 \text{ W m}^{-2}$ , is of the order of the difference between Maykut's calculations of  $F_c$  on the first day of March and April. Hence the spatial variability in  $F_c$  may be as important as the monthly time variation.

It is common to estimate the oceanic heat flux  $F_w$  as the difference between  $F_c$  and  $\overline{F}_\ell$ . In studies of thick perennial sea ice for which the oceanic heat flux near the ice/ocean interface is unaffected by solar radiation, such a method compares favorably with direct oceanographic measurements [Omstedt and Wettlaufer, 1992]. However, in the case of thin ice, solar insolation is a major factor in the heat budget of the upper ocean, and during LeadEx the effect was responsible for a strong diurnal variation in  $F_w$  from  $-50 \text{ W m}^{-2}$  during daylight to  $+50 \text{ W m}^{-2}$  in the evening when the radiative heat absorbed by the mixed layer escapes to the atmosphere [McPhee and Stanton, 1996; Morison and MCPhee, 1998]. Naive application of the residual method, wherein  $F_w = F_c - \overline{F}_\ell$ , yields Figure 6a, where we plot estimates derived from the temperature data from buoy 5 (dotted line) and buoy 6 (solid line) at lead 3. In Figure 6b we plot the residual flux estimates derived from the temperature data from buoy 6 with  $F_c$  calculated at the surface ( $z = 0$ ), at the ice center ( $z = 0.5h$ ) and at three quarters of the depth ( $z = 0.75h$ ). Because the volume fraction of liquid increases with depth, the conductive heat flux decreases

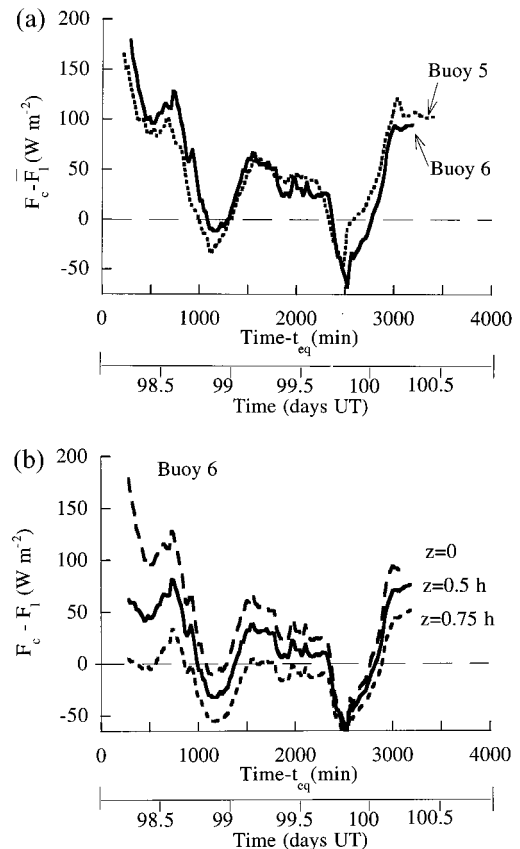


**Figure 6.** (a) Plot of the residual flux estimates ( $F_c - \overline{F}_\ell$ ) derived from the temperature data from buoy 5 (dotted line) and buoy 6 (solid line) at lead 3. (b) Plot of the residual flux estimates ( $F_c - \overline{F}_\ell$ ) derived from the temperature data from buoy 6 for which  $F_c$  is calculated at the surface ( $z = 0$ ), at the ice center ( $z = 0.5h$ ) and at three quarters of the depth ( $z = 0.75h$ ).

with depth and the magnitude of the residual is reduced. If we interpret  $F_c - \overline{F}_\ell$  as an estimate of  $F_w$ , then the time evolution and the sign of the residual are commensurate with direct oceanographic measurements made by *Morison and McPhee* [1998] and *McPhee and Stanton* [1996]. The magnitude of the residual for  $F_c$  estimated between  $z = 0.5h$  and  $z = 0.75h$  is commensurate with their oceanographic measurements of  $F_w$ . The depth dependence of oceanographic measurements taken in the water column leads to the interpretation that during the diurnal cycle the solar radiation absorbed in the upper few meters of the ocean during daylight resulted in a downward flux of heat by turbulent mixing. Therefore the residual method can yield a negative oceanic heat flux during intervals when the ice is actually growing. The dominant local energy balance between heat conduction and latent heat production is as if it were growing from a supercooled ocean, but the latter effect is entirely due to the solar heating of the mixed layer surface rather than through compositional supercooling. During the evening, the heat stored in the mixed layer is lost through the ice by heat conduction, and a positive residual is associated with ice growth and hence positive oceanic heat flux. Although during periods of negative oceanic heat flux the growth rate is nearly constant, latent heat flux drops because of the decrease in the solid fraction caused by the solar heating of the ice. Clearly, without independent heat flux measurements in the water column the residual method applied to thin ice without a proper accounting of the solid fraction evolution can be substantially misleading.

## 6. Salinity Fluxes

Observations and simulations broadly distinguish the regimes of lead convection as follows: during quiescent periods, haline convection is cellular, but when the wind-driven ice drift is strong, the oceanic boundary layer is fully turbulent [*Morison et al.*, 1992; *Smith and Morison*, 1993, 1998]. Laboratory experiments designed to study the role of rotation in turbulent convection are good analogues for convection in leads [see, e.g., *Maxworthy*, 1997, and references therein], and computer simulations [see, e.g., *Smith and Morison*, 1993] can vary lead width, drift speed, and buoyancy flux with relative ease. These approaches and the LeadEx field observations confirm that haline convection under leads is variable and intermittent. For example, the simulations of *Smith and Morison* [1993] show that as the lead width increases, the time period for plume generation decreases. *McPhee* [1994] has observed that under a convecting lead the mixing length increases linearly with depth in the upper 5 m. Hence even an accurate prediction of when brine release into the underice viscous sublayer occurs does not lead to a detailed prediction of how this signal will be observed directly in the ocean with the fixed mast, profiling, and autonomous vehicle (horizontal profiling) techniques. Indeed, direct measurements of salt flux in the oceanic boundary layer have only recently been achieved [*McPhee*, 1994], and the statistics of the near-surface and mixed layer turbulent boundary layer structure are complicated by many factors making intercomparison of different measurement techniques an ongoing research effort [*McPhee and Stanton*, 1996; *Morison and McPhee*, 1998; *McPhee*, 1998].

In order to obtain a general understanding of the relationship between the two-phase nature of sea ice and the buoyancy flux associated with its growth we performed laboratory experiments in which aqueous salt solutions were cooled and solid-

ified from above in an apparatus in which the mass balance was closed [*Wettlaufer et al.*, 1997a, b]. Qualitatively similar experiments were performed by *Voropayev and Fernando* [1999] in which the mass balance was not closed. Over a range of salinities ranging from a third to 4 times that of Arctic Surface Water, our solutions froze in the same manner as natural sea ice, forming a matrix of ice crystals and interstitial brine. As described above, such two-phase, two-component regions are generally called mushy layers, and they occur during directional solidification in many systems ranging from industrial to natural. In a series of experiments in which we varied the initial and boundary conditions we measured the salinity of the liquid region and the solid fraction of the mushy layer as a function of its thickness. Initially, in all experiments the salinity flux was zero, indicating that the dense brine which was formed remained confined to the mushy layer. However, convection of brine from the interior of the mushy layer began abruptly once the depth of the layer exceeded a critical value  $h_c$ . The experiments thus allowed us to determine the parameters controlling this value. Once  $h_c$  has been exceeded, the salinity flux increases with the thermal driving for solidification (essentially, the temperature drop across the layer). However, the flux and the thermal driving are not directly proportional since the flux is influenced in a nonlinear fashion by the changing permeability of the mushy layer. Moreover, the critical thickness increases with the thermal driving so that the salinity flux is essentially zero for longer. This is a consequence of the fact that when the thermal driving is greater, the resultant solid fraction of the mushy layer is larger. Hence its permeability is lower, and therefore its resistance to flow is greater. Finally, the return flow driven by the abrupt onset of salinity flux penetrates deep within the mushy layer [*Worster*, 1997; *Worster and Wettlaufer*, 1997] and gives rise to local solidification and melting, creating “brine channels” which are the principal path for brine drainage from the mushy layer. These mechanisms are basic to the heat and mass transfer in two-phase, two-component regions and have been confirmed by the theoretical description that brine expulsion is initially determined by a critical Rayleigh number for the mushy layer:

$$Ra = g\beta\Delta S\Pi(\bar{\phi})h/\kappa\nu, \quad (12)$$

which measures the driving buoyancy of the enriched brine relative to the resistance of the solid matrix. This Rayleigh number must exceed a critical value before significant drainage of interstitial brine can occur. In this definition,  $g$  is the acceleration due to gravity,  $\beta\Delta S = \beta(S_0 - S_f)$  is the difference in the liquid density across the mushy layer, where  $S_0$  is the initial salinity of the liquid region and  $S_f$  is the equilibrium salinity corresponding to the observed surface temperature,  $h$  is the thickness of the layer,  $\kappa$  and  $\nu$  are the thermal diffusivity and kinematic viscosity of the liquid, and  $\Pi$  is the permeability of the layer, which is a function of the solid fraction  $\bar{\phi}$ . The existence of a critical value of  $Ra$  indicates that the scaling relationship

$$(h_c\Delta S)^{-1} \propto \Pi(\bar{\phi}_c) \quad (13)$$

will be satisfied, where  $h_c$  is the critical thickness and  $\bar{\phi}_c$  is the value of the solid fraction measured at the critical time. Indeed, we found that all of our experimental data, spanning a wide range of initial salinities and surface temperatures, collapsed onto a curve described by this scaling relationship. This collapse is shown as the solid line in Figure 7a.

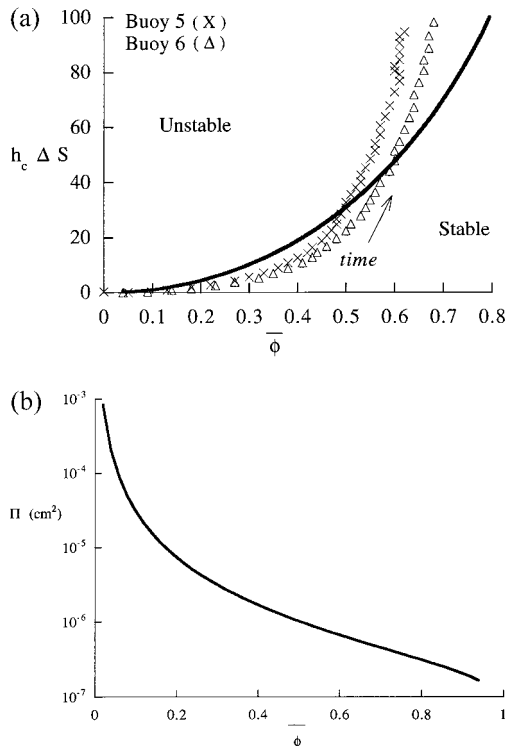


**Figure 7.** (a) The critical conditions for the onset of internally driven compositional convection expressed in terms of the solid fraction  $\bar{\phi}$  and the quantity  $h\Delta S$ . The solid line is a marginal stability curve derived from the theoretical collapse to equation (13) of a suite of laboratory data for the abrupt onset of brine flux out of a mushy layer, and the symbols denote buoy-derived values. The ice monitored by buoy 5 crosses the curve at  $\sim 350$  min when it is  $\sim 3.3$  cm thick, and that at buoy 6 crosses the curve at  $\sim 450$  min when it is  $\sim 3.6$  cm thick. The release occurs at  $\sim 98.3$  UT, which is very close to the time at which the first peak in the buoyancy flux at lead 3 was observed by McPhee, using one type of direct oceanographic measurement [McPhee and Stanton, 1996]. (b) An alternative interpretation of Figure 7a vis-à-vis equation (7) in which the effective permeability  $\Pi(\bar{\phi})$  corresponding to marginal stability conditions along the solid line in Figure 7a is plotted as a function of the solid fraction. Hence the effective permeability of sea ice is extracted from the values of  $\bar{\phi}$ , where the buoy data cross the marginal stability curve. The values of  $\Pi(\bar{\phi})$  are between  $10^{-6}$  and  $10^{-7}$  cm<sup>2</sup>, which are consistent with other observations.

We interpret the critical porous-medium Rayleigh number criterion as a marginal stability curve. Hence the dense brine in a mushy layer with a solid fraction and  $h\Delta S$  to the right of the curve will remain trapped within the interstices. However, when these values cross over the curve, brine is convected out of the mushy layer. To test when natural sea ice suffers this instability, we also plotted the buoy-derived values of  $\bar{\phi}$  and  $h\Delta S$  on Figure 7a. As time progresses,  $\bar{\phi}$  increases, but so too does the drive for convection out of the sea ice, described by  $h\Delta S$ . The trajectories for both buoys do indeed cross over the marginal stability curve under conditions remarkably similar to those we observed in the laboratory. The ice monitored by buoy 5 crosses the curve at  $\sim 350$  min when it is  $\sim 3.3$  cm thick, and that at buoy 6 crosses the curve at  $\sim 450$  minutes when it is  $\sim 3.6$  cm thick. The slightly higher solid fraction of the latter required a greater interstitial density contrast before the brine

could be released. The timing of the release between the buoys is also remarkably similar, occurring at  $\sim 98.3$  UT. This is very close to the time at which the first peak in the buoyancy flux at lead 3 was observed by McPhee using direct measurements of the ensemble average turbulent salinity flux [see McPhee and Stanton, 1996, Figure 16c]. Indirect estimates of the buoyancy flux from the dissipation of turbulent kinetic energy using T. Stanton's (personal communication, 1999) microstructure profiling instrument do not reveal the same peak. An examination of the origins of this apparent inconsistency is currently being undertaken (M. McPhee and T. Stanton, personal communication, 1999). We associate the peak in the buoyancy flux observed by McPhee with the sea ice at these locations reaching its critical porous-medium Rayleigh number.

As described above, the permeability of sea ice depends on its solid fraction, and our theory provides a description of this dependence. When we plot  $(h_c\Delta S)^{-1}$  versus critical liquid fraction  $(1 - \bar{\phi}_c)$  for all the experiments [Wettlaufer et al., 1997a, b], the trend of the function is consistent with the expected form of the permeability function, namely, that the permeability increases with the liquid fraction and has positive curvature, increasing rapidly as the liquid fraction approaches unity. An alternative interpretation of Figure 7a vis-à-vis equation (7) is shown in Figure 7b. The marginal stability conditions for convection of brine from the interior of the mushy layer assumes that the permeability is isotropic. Clearly, sea ice is an orthotropic material, but to deal with a tensor permeability function in the context of interpretation of field data is unwarranted. Theoretical calculations show that the critical porous-medium Rayleigh number  $Ra_c$  varies by approximately a factor of 2 over a wide range of control parameter space and a representative value is 10 [see Worster, 1992b, Figure 11]. This allows us to estimate the effective permeability of sea ice  $\Pi(\bar{\phi})$  from the values of  $h\Delta S$  along the marginal stability line of Figure 7a. We extract the values from the field observations by observing where the buoy data cross the marginal stability curve and find that  $\Pi(\bar{\phi})$  lies between  $10^{-6}$  and  $10^{-7}$  cm<sup>2</sup>, which is consistent with other observations [Saeki et al., 1986; H. Eicken, personal communication, 1999].

To further pursue the relationship between the permeability of the ice and the buoyancy flux at lead 3 as observed by direct oceanographic measurements, we plot the time evolution of

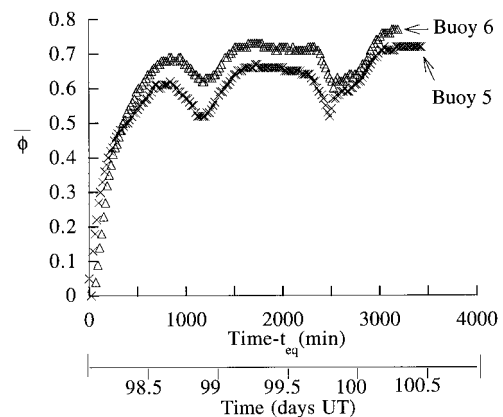


**Figure 8.** Time series of the solid fraction as derived from both buoys and applying equation (6) under the assumption of a linear temperature profile. As  $\bar{\phi}$  decreases,  $\Pi(\bar{\phi})$  increases and can initiate another release of brine into the mixed layer.

the solid fraction for both buoys in Figure 8. Note the two striking drops in the evolution of  $\bar{\phi}$  beginning at  $\sim 98.6$  UT and  $99.7$  UT. These are clearly associated with the diurnal radiative heating (Figure 2), but additionally, the associated reduction in the permeability can initiate another release of brine into the mixed layer. Indeed, the second and largest peak in the buoyancy flux occurred at  $\sim 98.7$  UT [see *McPhee and Stanton*, 1996, Figure 16]. (Their time series does not extend past  $99$  UT, so we are not able to investigate the correlation between the second drop in the permeability at  $99.7$  UT.)

## 7. Discussion

An important issue that we can address concerns the boundary conditions used in numerical models. As we have discussed above, although ice growth is continuous, the brine flux is not directly proportional to the growth rate for all stages of growth, although the latter has generally been supposed. The latter supposition is reasonable under the assumption that one knows the brine content of the ice being formed. Such a situation is not reached until after the onset of the instability that triggers the release of intercrystalline brine, a delay which can be greater than half an inertial period which is a significant portion of the duration of (1) a deployment at a lead, (2) current numerical simulations of lead induced thermohaline convection, and (3) the atmospheric heat signature associated with ice growth in a lead. In addition, abrupt changes in the thermal forcing can induce significant changes in the permeability of the ice that release brine into the mixed layer. Hence, quite independent of the turbulence in the mixed layer, the ice itself can be a significant source of intermittency in buoyancy flux.

Haline convection induced by ocean freezing occurs on characteristic scales that are smaller than most GCM grid cells, and hence, although large-scale models are very sensitive to the treatment of salt rejection during ice growth [e.g., *Duffy et al.*, 1999], an important question concerns how best to incorporate lead scale studies into GCM-scale simulations. Typical lead-scale simulations have a duration of several inertial periods. For example, *Smith and Morison's* [1993] two-dimensional hydrostatic model runs for two inertial periods. Their nonhydrostatic simulations run for half an inertial period [*Smith and Morison*, 1998]. The critical thickness from our field observations is reached in approximately three quarters of an inertial period. As discussed above, there are edge effects in the growth of lead ice, and these boundary regions will reach the critical thickness at earlier times. The major fraction of the ice area is much less thick and evolves in a manner more like our field observations. Because the numerical models do not treat the ice edge effects in terms of spatial variation in buoyancy forcing, the entire width of a simulated lead should possess a buoyancy forcing that is in accordance with the field and laboratory measurements which show a delayed flux over a time-scale that is of order the simulation time. Once the release occurs, the qualitative features of the simulations may be of some guidance. Plumes are released in a transient manner at the trailing edge of the lead. Their subsequent downstream evolution, perhaps including breakup, is essentially what is being measured by the fixed mast and vertical profiling instruments of *McPhee and Stanton* [1996].

Finally, two other implications deserve comment. First, the importance of young sea ice combined with its inaccessibility motivate refinement of remote-sensing techniques that can resolve dielectric contrasts on length scales of tens of centime-

ters [*Winebrenner et al.*, 1995]. The leading-order contribution to electromagnetic volume scattering originates from the brine volume profile, and therefore our studies of the time evolution of the solid fraction link the analysis of radar backscatter data to the basic phase behavior of a growing ice sheet. We note further that an increase in salinity of the upper surface of sea ice is observed [*Perovich and Richter-Menge*, 1994; *Martin et al.*, 1996], and this strongly influences the brightness temperature of young sea ice. However, the dynamics of this process, while certainly influenced by mushy layer convection, is probably largely dominated by solute-enhanced thermomolecular pressure-driven transport along interfacial films [see, e.g., *Wetlaufer*, 1998]. The important linkage between the phase fraction of sea ice and its dielectric structure, while part of our research program, is not the focus of this paper. Second, our basic treatment of sea ice as a mushy layer should be useful as a predictive tool for stable isotope fractionation processes that occur during growth. This topic has been addressed in the context of the analysis of ice cores taken from the Weddell Sea [*Eicken*, 1998], in which, relative to young Arctic sea ice, a substantial fraction is of a granular texture. Therefore the largely columnar structure of young Arctic sea ice lends itself to laboratory and theoretical studies along these lines.

In summary, through a detailed analysis of traces of temperature against time taken from specially designed buoys, we have found several basic mechanisms of the dynamics of mushy layers to be operating during the natural solidification of leads. First, we have made a quantitative connection between a critical porous-medium Rayleigh number, which delineates the stability criterion between trapping of brine within the sea ice matrix and convection of brine out of the interstices and into the mixed layer and direct measurements of the oceanic buoyancy flux. The approach provides an estimate of the effective permeability of young sea ice. Second, we have found an additional correlation between radiatively induced increases in the sea ice permeability and salinity-induced buoyancy flux in the ocean. Therefore independent of the turbulence in the mixed layer, the ice itself can be a significant source of intermittency in buoyancy flux. The analysis has shown the important influence that a proper treatment of the phase evolution of sea ice has on the heat balance during the early stages of ice growth in leads. We believe that the concepts presented here will be of general use in future numerical modelling studies, laboratory experiments, and analysis of field data.

**Acknowledgments.** J.S.W. would like to thank colleagues from the LeadEx Group for the cooperative effort that made the scientific and logistical difficulties of the program progress smoothly. Andreas Heiberg, John Bitters, and Jamie Morison were responsible for the success of the daunting logistical challenge, and Tom Curtin has patiently awaited the results. Discussions and exchanges on the manuscript with Miles McPhee, Tim Stanton, Tony Maxworthy, Jamie Morison, and Willy Weeks are gratefully acknowledged, as are discussions with Hajo Eicken concerning sea ice permeability. Russ Light was of crucial help with some in-field computer programming, and Bill Hanot and Dan Stearns were the primary electrical and mechanical engineers, respectively. David Morison and Andrew Roach wrote software to convert and analyze some of the data for which we are very grateful. We are pleased to acknowledge the support provided for this work by the U.S. Office of Naval Research and National Science Foundation and the British Natural Environment Research Council.

## References

Badgley, F. I., Heat budget at the surface of the Arctic Ocean, in *Proceedings of the Symposium on the Arctic Heat Budget and Atmo-*

- spheric Circulation*, edited by J. O. Fletcher, pp. 267–278, Rand Corp., Santa Monica, Calif., 1966.
- Cox, G. F. N., and W. F. Weeks, Numerical simulations of the profile properties of undeformed first-year sea ice during the growth season, *J. Geophys. Res.*, *93*, 12,449–12,460, 1988.
- Duffy, P. B., M. Eby, and A. J. Weaver, Effects of sinking of salt rejected during formation of sea ice on results of an ocean-atmosphere-sea ice climate model, *Geophys. Res. Lett.*, *26*, 1739–1742, 1999.
- Eicken, H., Deriving modes and rates of ice growth in the Weddell Sea from microstructural, salinity and stable-isotope data, in *Antarctic Sea Ice: Physical Processes, Interactions, and Variability*, *Antarct. Res. Ser.*, vol. 74, edited by M. O. Jeffries, pp. 89–122, AGU, Washington, D. C., 1998.
- Gow, A. J., D. A. Meese, D. K. Perovich, and W. B. Tucker III, The anatomy of a freezing lead, *J. Geophys. Res.*, *95*, 18,221–18,232, 1990.
- Gross, G. W., A. Gutjahr, and K. Caylor, Recent experimental work on solute redistribution at the ice/water interface: Implications for electrical properties and interface processes, *J. Phys. Colloq.*, *48*(C1), 527–533, 1987.
- Kurz, W., and D. J. Fisher, *Fundamentals of Solidification*, Trans. Tech. Publ., Rockport, Mass., 1984.
- Malmgren, F., On the properties of sea ice, in *The Norwegian Polar Expedition 'Maud,' 1918–1925, Scientific Results*, vol. 1a(5), pp. 1–67, 1927.
- Martin, S., Y. Yu, and R. Drucker, The temperature dependence of frost flower growth on laboratory sea ice and the effect of the flowers on infrared observations of the surface, *J. Geophys. Res.*, *101*, 12,111–12,125, 1996.
- Maxworthy, T., Convection into domains with open boundaries, *Annu. Rev. Fluid Mech.*, *29*, 327–371, 1997.
- Maykut, G. A., Energy exchange over young sea ice in the central Arctic, *J. Geophys. Res.*, *83*, 3646–3654, 1978.
- Maykut, G. A., Large-scale heat exchange and ice production in the central Arctic, *J. Geophys. Res.*, *87*, 7971–7984, 1982.
- McPhee, M. G., On the turbulent mixing length in the oceanic boundary layer, *J. Phys. Oceanogr.*, *97*, 2014–2031, 1994.
- McPhee, M. G., An inertial-dissipation method for estimating turbulent flux in buoyancy-driven, convective boundary layers, *J. Geophys. Res.*, *103*, 3249–3255, 1998.
- McPhee, M. G., and T. P. Stanton, Turbulence in the statically unstable boundary layer under Arctic leads, *J. Geophys. Res.*, *101*, 6409–6428, 1996.
- Morison, J. H., and M. G. McPhee, Lead convection measured with an autonomous underwater vehicle, *J. Geophys. Res.*, *103*, 3257–3281, 1998.
- Morison, J. H., and J. D. Smith, Seasonal variations in the upper Arctic Ocean as observed at T-3, *Geophys. Res. Lett.*, *8*, 753–756, 1981.
- Morison, J. H., M. G. McPhee, T. B. Curtin, and C. A. Paulson, The oceanography of winter leads, *J. Geophys. Res.*, *97*, 11,199–11,218, 1992.
- Omstedt, A., and J. S. Wettlaufer, Ice growth and oceanic heat flux: Models and measurements, *J. Geophys. Res.*, *97*, 9383–9390, 1992.
- Perovich, D. K., and J. A. Richter-Menge, Surface characteristics of lead ice, *J. Geophys. Res.*, *99*, 16,341–16,350, 1994.
- Saeki, H., T. Takeuchi, M. Sakai, and E. Suenaga, Experimental study on permeability coefficient of sea ice, in *Proceedings of International Conference on Ice Technology*, pp. 237–246, Springer-Verlag, New York, 1986.
- Smith, D. C., IV, and J. H. Morison, A numerical study of haline convection beneath leads in sea ice, *J. Geophys. Res.*, *98*, 10,069–10,083, 1993.
- Smith, D. C., IV, and J. H. Morison, Nonhydrostatic haline convection under leads in sea ice, *J. Geophys. Res.*, *103*, 3233–3247, 1998.
- The LeadEx Group, The LeadEx experiment, *Eos Trans. AGU*, *74*(35), 393, 396–397, 1993.
- Untersteiner, N., On the mass and heat budget of arctic sea ice, *Arch. Meteorol. Geophys. Bioklimatol.*, Ser. A, *12*, 151–182, 1961.
- Voropayev, S. I., and H. J. S. Fernando, Evolution of two-layer thermohaline systems under surface cooling, *J. Fluid Mech.*, *380*, 117–140, 1999.
- Weeks, W. F., Growth conditions and the structure and properties of sea ice, in *Physics of Ice-Covered Seas*, edited by M. Leppäranta, pp. 25–104, Univ. of Helsinki Press, Helsinki, 1998.
- Wettlaufer, J. S., Introduction to crystallization phenomena in sea ice, in *Physics of Ice-Covered Seas*, edited by M. Leppäranta, pp. 105–194, Univ. of Helsinki Press, Helsinki, 1998.
- Wettlaufer, J. S., M. G. Worster, and H. E. Huppert, The phase evolution of young sea ice, *Geophys. Res. Lett.*, *24*, 1251–1254, 1997a.
- Wettlaufer, J. S., M. G. Worster, and H. E. Huppert, Natural convection during solidification of an alloy from above with application to the evolution of sea ice, *J. Fluid Mech.*, *344*, 291–316, 1997b.
- Winebrenner, D. P., L. D. Farmer, and I. R. Joughin, On the response of polarimetric synthetic aperture radar signatures at 24-cm wavelength to sea ice thickness in Arctic leads, *Radio Sci.*, *30*, 373–402, 1995.
- Worster, M. G., The dynamics of mushy layers, in *Interactive Dynamics of Convection and Solidification*, *NATO ASI Ser.*, Ser. E, vol. 219, edited by S. H. Davis et al., pp. 113–138, Kluwer Acad., Norwell, Mass., 1992a.
- Worster, M. G., Instabilities of the liquid and mushy regions during solidification of alloys, *J. Fluid Mech.*, *237*, 649–669, 1992b.
- Worster, M. G., Convection in mushy layers, *Annu. Rev. Fluid Mech.*, *29*, 91–122, 1997.
- Worster, M. G., and J. S. Wettlaufer, Natural convection, solute trapping and channel formation during solidification of saltwater, *J. Phys. Chem. B*, *101*, 6132–6136, 1997.

H. E. Huppert and M. G. Worster, Institute of Theoretical Geophysics, Department of Applied Mathematics and Theoretical Physics, University of Cambridge, Silver Street, Cambridge CB3 9EW, England. (heh1@esc.cam.ac.uk; grae@esc.cam.ac.uk)

J. S. Wettlaufer, Applied Physics Laboratory, University of Washington, Box 355640, Seattle, WA 98105. (wett@apl.washington.edu)

(Received January 8, 1999; revised August 10, 1999; accepted October 4, 1999.)